HHS Public Access

Author manuscript

Sci Transl Med. Author manuscript; available in PMC 2019 March 12.

Published in final edited form as:

Sci Transl Med. 2014 December 03; 6(265): 265ra167. doi:10.1126/scitranslmed.3009500.

PET/CT monitoring demonstrates a therapeutic response to oxazolidinones in *Mycobacterium tuberculosis*-infected macaques and humans

M. Teresa Coleman[1], **Ray Y. Chen**[2], **Myungsun Lee**[3], **Philana Ling Lin**[4], **Lori E. Dodd**[5], **Pauline Maiello**[1], **Laura E. Via**[2], **Youngran Kim**[3], **Gwendolyn Marriner**[2], **Veronique Dartois**[6], **Charles Scanga**[1], **Christopher Janssen**[7], **Jing Wang**[8], **Edwin Klein**[7], **Sang Nae Cho**[3,9], **Clifton E. Barry III**[2,10,*], and **JoAnne L. Flynn**[1,*]

[1]Department of Microbiology and Molecular Genetics, University of Pittsburgh School of Medicine, Pittsburgh, PA, USA

[2]Tuberculosis Research Section, Laboratory of Clinical Infectious Diseases, NIAID, NIH, Bethesda, MD, USA

[3]International Tuberculosis Research Center, Changwon, Republic of Korea

[4]Department of Pediatrics, Children's Hospital of Pittsburgh of the University of Pittsburgh Medical Center, Pittsburgh, PA, USA

[5]Biostatistics Research Branch, NIAID, NIH, Bethesda, MD, USA

[6]PHRI Center, Rutgers New Jersey Medical School, Newark, NJ, USA

[7]Division of Laboratory Animal Resources, University of Pittsburgh, Pittsburgh, PA, USA

[8]Clinical Research Directorate/Clinical Monitoring Research Program, Leidos Biomedical Research, Inc., Frederick National Laboratory for Cancer Research, Frederick, MD, USA

[9]Department of Microbiology, Yonsei University College of Medicine, Seoul, Republic of Korea

[10]Institute of Infectious Disease and Molecular Medicine, and the Department of Clinical Laboratory Sciences, Faculty of Health Sciences, University of Cape Town, Rondebosch, South Africa

Abstract

Oxazolidinone antibiotics such as linezolid have shown significant therapeutic effects in patients with extensively drug-resistant (XDR) tuberculosis (TB) despite modest effects in rodents and no demonstrable early bactericidal activity in human Phase 2 trials. Here, we show that monotherapy with either linezolid or AZD5847, a second-generation oxazolidinone, reduced bacterial load at necropsy in *Mycobacterium tuberculosis*-infected cynomolgus macaques with active TB. This

*To whom correspondence should be addressed: cbarry@niaid.nih.gov, joanne@pitt.edu.

Author contributions: MTC, PLL, PM, CS, CJ, EK and JLF designed and performed all NHP experiments; MTC, RYC, LD, PM, and CEB performed analysis of radiology data; RYC, ML, LV, SNC and CEB designed and implemented the PET/CT substudy in the LZD clinical trial; GM and VD synthesized standards and supervised NHP for PK study design and sample analysis; LD, JW and PM performed statistical analyses.

Competing interests: The authors declare no competing interests.

effect coincided with a decline in FDG PET imaging avidity in the lungs of these animals and with reductions in pulmonary pathology measured by serial CT scans over two months of monotherapy. In a parallel Phase 2 clinical study of linezolid in patients infected with XDR-TB, we also collected PET/CT imaging data from subjects receiving linezolid that had been added to their failing treatment regimens. Quantitative comparisons of PET/CT imaging changes in these human subjects were similar in magnitude to those observed in macaques, demonstrating that the therapeutic effect of these oxazolidinones can be reproduced in this model of experimental chemotherapy. PET/CT imaging may be useful as an early quantitative measure of drug efficacy against TB in human patients.

Single Sentence Summary:

PET/CT imaging in macaques and humans with TB shows a beneficial therapeutic response to linezolid and a new oxazolidinone antibiotic AZD5847.

Editor's Summary:

Visualizing Drug Responses in TB

A pair of papers by Chen *et al.* and Coleman *et al.* investigate how changes in quantitative PET/CT scans in both nonhuman primates and humans can be used as early surrogate markers of treatment efficacy in tuberculosis. The Coleman *et al.* study shows that treatment of *Mtb*-infected macaques with linezolid and the second-generation oxazolidinone AZD5847 resulted in a reduced bacterial load at necropsy and reduced FDG PET avidity and CT-quantified lung pathology. Similar PET/CT changes were seen in human patients infected with extensively drug-resistant *Mtb* and treated with linezolid. The companion study by Chen *et al.* corroborated this effect in a prospective analysis of patients with multidrug-resistant tuberculosis and demonstrated that early PET/CT changes predicted final treatment outcomes.

Introduction

Tuberculosis (TB) is a devastating disease afflicting an estimated 8.6 million people in 2012 (1). Even chemotherapy for drug-sensitive disease is complex, requiring 6–8 months of treatment with four different agents to achieve a durable cure. If patients fail first-line therapy and develop multidrug-resistant (MDR) TB, a full two years of chemotherapy with as many as six different agents is required (2). Of the nearly 500,000 incident cases of MDR TB globally, only about one-fifth were detected and only 77,000 received treatment in 2012. Given this situation, it is unsurprising that 170,000 of the estimated 1.3 million deaths from TB in 2012 were due to MDR disease (1). Treatment success for MDR TB globally is estimated to be only 50%, which increases the risk for the development of extensively drug-resistant (XDR) TB where the prognosis becomes even poorer. Because of the difficulty in treating such patients, the US Centers for Disease Control listed XDR-TB as one of the top five global infectious disease threats last year (3).

One of the major difficulties in managing TB is the lengthy nature of treatment regimens, and shortening treatment duration is an important goal of many on-going efforts. Treatment duration has been determined empirically by randomized clinical trials comparing disease

relapse following treatments of different durations, often motivated primarily by results in animal models of experimental chemotherapy. Mouse models of disease have been used virtually exclusively to justify exposing patients to the risk of a shortened duration of chemotherapy (4). The standard murine disease models, however, develop none of the characteristic pathology of TB disease such as the formation of cavities in the lungs, which in human clinical trials are known to be strongly correlated with failure and disease relapse [reviewed in (5)], nor lesions with caseous necrosis, which are the most common lesions in human TB. Several large Phase 2 and 3 treatment shortening trials have been attempted based upon predictions made in murine models, with disappointing results leading to concerns regarding the predictive validity of this model (6, 7).

The lack of advanced pathology in murine TB also affects the local environment experienced by the bacilli and differences in this environment can affect the intrinsic drug susceptibility of the organism. In humans, there is a broad spectrum of lesions with bacteria found both extracellularly and intracellularly within many cell types, whereas in the mouse it is primarily a disease of the pulmonary macrophages (8, 9). In addition, murine pharmacokinetic (PK) profiles are often distinct from human profiles. Drugs are more rapidly metabolized requiring comparisons between profiles that have different peak drug concentration and half-lives. Recently, we reported a Phase 2 clinical study of linezolid (LZD) in chronically infected patients with XDR TB (10). The study added LZD to a failing regimen that each patient had been on for at least the previous six months, evaluating the effect of LZD essentially as monotherapy. LZD treatment was highly effective, with 87% of these patients ultimately having TB-free sputum cultures with a median time to conversion of 76 days of therapy. This result was surprising because LZD has only modest effects in murine models of TB, yet culture conversion rates approached those seen in standard five drug combination regimens used to treat MDR TB. Considered together, these studies suggest that murine models of disease inadequately measure the effect of this drug class in human disease.

Despite the beneficial effect of LZD reported in XDR TB patients, long-term administration of this agent is associated with significant side effects; in our study 82% of participants experienced clinically significant adverse events. Linezolid is the first in class of oxazolidinone antibiotics whose mechanism involves inhibition of bacterial protein synthesis through binding to the 50S subunit of the bacterial ribosome (11). Some of the side effects seen with LZD are a consequence of incidental binding to the human mitochondrial ribosome (12). Knowledge of this mechanism of toxicity has invigorated a search for new oxazolidinones with an improved safety profile. Several candidates that may offer such an advantage have been identified and are in clinical trials for TB or other indications (13, 14). One of these second-generation LZD analogs is AZD5847, a new oxazolidinone that has comparable activity to LZD against TB, both in vitro and in macrophages (15, 16).

We have developed TB chemotherapy models in two species of non-human primates to determine the efficacy of agents for treatment of both latent and active disease (17–19). The cynomolgus macaque develops TB disease that is strikingly similar to human disease (20, 21). Here, we show that macaques have a similarly strong therapeutic response to treatment with oxazolidinones as seen in humans in terms of reduced bacterial burden after treatment.

We also report similar radiologic responses in both human subjects from our previous trial (ClinicalTrials.gov #NCT00727844) and this non-human primates species over time using 2-deoxy-2-[^{18}F]-fluoro-D-glucose (FDG) positron emission tomography/computed tomography (PET/CT) imaging.

Results

Pharmacokinetics of linezolid and AZD5847 in cynomolgus macaques

To identify the doses of linezolid and AZD5847 that reproduce drug exposure in humans, pharmacokinetic (PK) dose finding studies were initially conducted in uninfected cynomolgus macaques. Linezolid was administered by oral gavage at 5 mg/kg, 10 mg/kg and 30 mg/kg to groups of three non-human primates, and blood was collected at serial time points from 0 to 36h post dose. Likewise, PK profiles were obtained from groups of three non-human primates that received AZD5847 at 10 mg/kg and 20 mg/kg by oral gavage. Relevant oral PK parameters are summarized in Table 1 and compared with human PK parameters observed either in TB patients treated with linezolid (22), or in human volunteers who received AZD5847 in a Phase 1 study of dose finding and tolerability (23, 24). These results indicated that in cynomolgus macaques a daily dose of 30 mg/kg of linezolid achieved peak plasma concentrations (C_{max}) and exposure (AUC, Area Under the Curve) comparable to those observed in TB patients (Table 1). For AZD5847, exposure did not increase between 10 and 20 mg/kg administered as single oral doses, but the terminal half-life was significantly longer at 20 mg/kg, suggesting saturation of one or more elimination processes. Multiple 20 mg/kg dose projections based on the single dose profile predicted an increase in exposure of 20–25% at steady-state. Therefore a daily dose of 20 mg/kg was selected to best reproduce C_{max} and exposure measured at one possible human dose of 400 mg twice daily (24). (The concentration-time profiles of linezolid at 30 mg/kg and AZD5847 at 10 and 20 mg/kg are presented in Fig. S1.)

To ensure that target drug concentrations were achieved in animals on treatment, blood samples were collected weekly at 6h post-dose during efficacy studies, i.e. each animal contributed 7 to 8 blood samples obtained once a week during the two-month period of daily treatment. Average linezolid concentrations at 6h post-dose ranged from 10 to 16 μg/ml, with inter-week standard deviations of 4.4 to 10.9 μg/ml within non-human primates. For AZD5847, average plasma concentrations at 6h ranged from 1.6 to 5.1 μg/ml, with inter-week standard deviations of 0.9 to 3.2 μg/ml. These drug concentrations confirmed the anticipated accumulation of AZD5847 at steady state compared to single dose, and were within the human-equivalent target range (Table 1), taking into consideration inter-animal and inter-occasion variability in the rate and extent of absorption.

To assess side effects of oxazolidinones, complete blood cell counts were performed on control and treated animals biweekly during treatment. Changes in white cell counts, hemoglobin, platelets or reticulocytes were not noticeably different from controls in the subset of animal monitored (Table S1).

Microbiological and pathological response to oxazolidinone treatment in non-human primates

Cynomolgus macaques were infected with *Mycobacterium tuberculosis* (Mtb) and monitored for progression to active disease, based on previously published criteria (18, 21). As with humans, macaques present with a wide range of disease severity. Non-human primates with active disease were subjected to a baseline PET/CT scan and randomly assigned to no treatment (n=9), LZD (30 mg/kg/day, n=5) or AZD5847 (20 mg/kg/day, n=6) groups and treated once daily for 2 months after which the animals were humanely euthanized. Pre-necropsy PET/CT scans were used as maps for obtaining individual tracked lesions, thoracic lymph nodes and other pathologies, and a pathologist blinded to the study scored the gross pathology based on a published scoring system (21). Tissue samples, including the majority of granulomas, all thoracic lymph nodes, all lung lobes including uninvolved tissue, and extrapulmonary sites (liver and spleen) were obtained for bacterial culture and histopathology, as previous described (18).

In previous work, we developed and validated a scoring system [colony forming unit (CFU) score] for estimating total bacterial burden in non-human primates (21), based on plating of all samples described above. This CFU score reflects a quantitative assessment of all visible lesions and all lymph nodes as well as samples from ostensibly healthy lung and is a reasonable estimate of total bacterial burden. We have shown in previous work that this score successfully discriminates effectively drug-treated animals from untreated controls in the cynomolgus macaque model (18). As expected with out-bred non-human primates, the active TB untreated controls had a wide range of bacterial burden at necropsy. CFU scores were significantly lower in the LZD-treated and AZD5847-treated groups ($p<0.01$ for both), compared to controls (Fig. 1A). As a means of assessing the ability of these agents to sterilize infected tissues, we calculated the percentage of all samples in each monkey that were positive for Mtb; untreated non-human primates had a higher proportion of samples that grew Mtb compared to either LZD ($p<0.01$) or AZD5847 ($p<0.05$) treated animals (Fig. 1B). We also quantified bacterial burden in individual lesions by plating each individual granuloma and thoracic lymph node obtained from each animal, and enumerated the actual number of bacilli per lesion. The median CFU from individual granulomas from active TB controls was significantly higher than the median CFU of individual granulomas from LZD- or AZD5847-treated animals ($p<0.001$ for both; Fig. 1C). The proportion of lesions that were sterile [i.e. no culturable bacilli, as defined previously (25)] from the LZD- or AZD5847-treated animals was also significantly higher than the proportion of sterile lesions in the granulomas of untreated animals ($p<0.05$ for both; Fig 1D). Finally, the bacterial burden in thoracic lymph nodes was significantly reduced in both the oxazolidinone treated groups compared to untreated animals ($p<0.001$ for AZD5847; $p<0.05$ for LZD; Fig. 1E). These data support that, as a single drug therapy, both oxazolidinones are capable of reducing overall bacterial burden and of sterilizing individual granulomas within 2 months of treatment.

CT responses in LZD- or AZD-treated non-human primates

Animals received PET/CT scans immediately prior to the initiation of chemotherapy, and after 4 or 8 weeks of treatment, with 8 weeks being immediately prior to necropsy. All three

scans for each animal were carefully co-registered, focusing on maximizing alignment of disease sites. Regions of interest were then manually delineated in the thoracic cavity on all three scans simultaneously, excluding lymph nodes, and the total disease-associated abnormal volume was computed. As with human TB patients, the macaques presented with a variable extent of disease ranging from <1 to 24 mL of volume between −500 and 200 Hounsfield Units [HU, a quantitative measure of radiodensity referenced to water (0) and air (−1000)]. Based on the correlation of reader scores observed in human CT scans (26), we analyzed these densities in two separate windows, a “soft” window between −500 and −100 HU that correlated more with nodular lesions and opacities and a “hard” window from −100 to +200 HU corresponding to consolidative features and cavity walls. For each subsequent scan we enumerated the $\log_2$-fold change in voxels of that density compared to the baseline volume.

Control animals primarily showed evidence of progressive disease in both windows while both treatment groups showed evidence of response to therapy at one month that increased in extent at two months (Fig. 2A, Fig. S2). Although the majority of disease (75–80%) was associated with soft lesion density, the resolution of hard features appeared more rapid and consistent. Both groups of treated animals showed quantitative reductions in disease density at a similar rate, suggesting roughly equal efficacy of these two agents in this model.

PET responses to LZD- or AZD-treatment in nonhuman primates

FDG uptake was quantified in co-registered scans from the entire thoracic cavity and enumerated as total glycolytic activity for each animal. As with CT abnormalities, a wide range of initial uptake was observed in these scans and untreated animals had a tendency to either remain unchanged in their total uptake of FDG or to show an increase, sometimes substantially (half the untreated animals experienced more than 50% increase in total glycolytic activity over the two month period) (Fig. 2B; Fig S3 shows examples of scans from individual animals on treatment). In contrast, treated animals exhibited mostly consistent reductions in FDG uptake. Combining all of the data from these animals, the total glycolytic activity was reduced by 2 months in oxazolidinone-treated animals, whereas an increase in total glycolytic activity was observed in untreated non-human primates (Fig. 5). In fact, there was a significant reduction in total glycolytic activity in both LZD- and AZD-treated animals as early as 1 month after starting treatment ($p<0.05$).

Dynamic PET changes in untreated patients with XDR TB

As a substudy within our Phase 2 clinical trial of the utility of LZD in treating subjects with chronic, non-responsive XDR-TB (10), we included subjects who were healthy enough to participate in an evaluation of the timing of PET/CT scanning in order to monitor their response to treatment with LZD. Nineteen of 41 subjects enrolled in the study consented to participate in this substudy (one subject was withdrawn after the baseline scan because s/he did not have XDR-TB). All subjects in the substudy received baseline scans immediately prior to receiving LZD as well as scans after receiving six months of LZD. All subjects also were randomly assigned to receive an additional scan at: (1) two months before starting LZD (delayed arm only, n=5); (2) one month after starting LZD (n=4); (3) two months after starting LZD (n=4); or (4) three months after starting LZD (n=5). According to this

schedule, each sub-study subject received a total of three scans up until six months of LZD treatment.

Five subjects enrolled in the delayed therapy arm of the main study received PET/CT scans upon enrollment and then immediately prior to receiving their first dose of study drug. Of these five, three showed slight increases in total glycolytic activity summed across their entire lungs on their second scan, whereas two stayed stable. Analysis of the lesions in these subjects, however, revealed remarkable changes in FDG uptake by individual lesions as illustrated by the example from one individual shown in Fig. 3A. This subject had a ten-year history of disease and his bacterial isolate was resistant to every available therapy but he had been maintained on isoniazid and levofloxacin for the six months prior to study entry and experienced no change in his failing regimen for the first two months per study protocol. Nonetheless this subject developed a new left lower lobe lesion near the heart while a middle lobe lesion near the mediastinum resolved. Over the same time period his sputum smear went from 2+ to 3+ on the internationally accepted standard semi-quantitative scale for grading the number of acid-fast bacilli present and the days to positivity of his BACTEC culture (an automated culture system widely used in clinical mycobacteriology) went from 28 to 15 consistent with a slight worsening of disease. This general pattern of local waxing and waning of lesions was observed in all five patients in this group (Fig S4 shows scans for the other four patients). Patients in this subgroup with an extensive and long history of disease showed evidence of both regressing and progressing lesions, new lesions, and newly infected lymph nodes in this short two-month interval prior to being treated with LZD. This level of dynamic change in individual lesions, against a backdrop of relatively constant overall disease in the lung, highlights the dynamic and local nature of TB lesions, similar to our data in macaques (21, 25).

PET changes in LZD-treated subjects

Upon starting LZD therapy, all but two subjects showed a consistent diminution of total glycolytic activity in their lungs by 6 months as shown in Figure 3B. Two other subjects had a transient increase in total glycolytic activity at the intermediate scan time point (one at month 1 and the other at month 2). An example of this rapid response to therapy is shown in Fig. 3A (compare the middle pre-LZD scan to the right scan at six months). A single subject showed a decrease in total glycolytic activity at one month followed by a doubling of FDG uptake at six months. Examination of the microbiologic response of this patient showed an initial improvement over the first two months in both smear and culture but by month 4 of treatment both had become positive again and the minimum inhibitory concentration (MIC) for LZD of bacilli isolated from his sputum went from 0.5 ug/ml at 12 weeks to 4 ug/ml at 21 weeks. Sequencing of the 23S ribosomal RNA gene from this patient's 21-week sputum *Mtb* isolate revealed a mixture of the wild type allele (G2576) and a mutant allele (G2576T). Sequencing of a sputum sample obtained at 53 weeks revealed only the mutant allele. Examination of this patient's entry scan showed bilateral apical disease including a large cavity in the left upper lobe that was the major site of metabolically active disease (Fig. 4). This cavity partially resolved at one month (Fig. 4, lower left) but on the six-month (24 week) scan a new anterior lesion appeared from the bottom of the initial cavity (Fig. 4, lower right shows the new lesion in red, Fig. S5 shows additional detail), which is therefore the

likely site of expansion of the LZD-resistant bacteria. Supplemental figure S8 shows PET and CT changes for the four LZD XDR-TB patients with PET/CT scans at 2 months relative to the PET/CT changes from the MDR-TB patients in the companion paper.

Comparative PET changes with oxazolidinone treatment across humans and nonhuman primates.

Averaging total glycolytic activity $\log_2$-fold changes from baseline to post-treatment time points across all human subjects who received scans at one, two and three months showed an overall response by 3 months (Fig. 5), allowing direct comparisons of the response magnitude to that observed in the macaques. The magnitude of the response seen in this non-human primate species to treatment with LZD was quantitatively similar to the response observed in human subjects (compare the dotted blue and solid blue lines in Fig. 5). The changes in CT volumes in these chronically infected subjects across the first three months were minimal; many of these subjects had extensive areas of FDG-cold but CT dense lesions that presumably reflected pathology from previously treated or less active areas of disease, highlighting the utility of measuring metabolic activity (Figs. S6A and B).

Discussion

LZD and AZD5847 appear to elicit similar therapeutic responses in non-human primates as measured by both bacteriological burden at necropsy and radiologic endpoints. This result stands at odds with reports in the literature that AZD5847 results in a substantially higher rate of killing of bacilli (1.5 $\log_{10}$ CFU/ml after ten days) than LZD (<0.5 $\log_{10}$ CFU/ml after ten days) in infected murine bone-marrow derived macrophages with a similar disparity seen in aerobic killing of *Mtb* (15). This differential sensitivity is not unexpected since Mtb in primates (human or non-human) is neither found exclusively within macrophages nor growing on rich media containing glucose and glycerol (9). It does, however, reinforce the importance of exploring models of experimental chemotherapy that more faithfully recapitulate the physiological state(s) of the bacterium and complex pathologies in humans when making predictions regarding their likely utility in the clinic.

These results support further clinical evaluation of AZD5847 since the efficacy of LZD in TB patients appears good (27–30). Since the primary concerns with wider usage of LZD revolve around safety issues, this newer oxazolidinone may well show less side effects. Future studies with AZD5847 should therefore focus on establishing the long-term safety of administration of this agent in TB patients.

This study was designed to allow a direct comparison of radiologic changes in human patients and non-human primates being treated effectively with oxazolidinone monotherapy. Human subjects recruited into this study were required to have a history of a stable, unchanging and failing regimen for the prior six months. At the time of LZD addition, no changes to this failing regimen were allowed per protocol. Changes were allowed after sputum smear conversion, based upon the results of comprehensive drug-susceptibility testing performed on their initial isolates. During the first two months of therapy, when PET/CT data for comparison was collected, no additional regimen changes were made, thus the changes in radiological features were likely to be due solely to the addition of LZD.

Although the subjects included in this study had experienced multiple rounds of failed chemotherapy, in general the extent of lung pathology is similar to primary disease albeit on the more severe end of the spectrum. PET reports on active areas of disease, which offers a significant benefit over structural imaging modalities like chest X-rays or CT in that it allows discrimination between active sites of disease and residual pathology from disease that has resolved. Although the small numbers of patients reported herein is a limitation, the fact that response rates by PET can be observed and quantified suggests that this imaging modality is an important adjunct to microbiological response rates that may improve the precision of early Phase 2 evaluations of new drugs and regimens. Our results corroborate the results reported in our companion paper (26). In that study, 28 subjects with pulmonary MDR-TB were treated with an optimized regimen for 24 months, then followed another 6 months for final treatment outcomes. PET/CT scans were conducted at baseline, and at 2 and 6 months and quantitative changes were correlated with final treatment outcomes at 30 months. The magnitude of PET/CT changes in the 4 LZD-treated subjects at 2 months was consistent with the decreased FDG avidity reported in that study, however these changes were less dramatic compared to the magnitude of changes from our companion study (Figs. S8A, B and C). This is not surprising as the LZD subjects had XDR-TB and effectively received only one active drug, whereas the companion study patients had MDR-TB and received an optimized regimen with 4 to 5 active drugs.

The correspondence in magnitude and timing of the PET/CT responses seen in these subjects was similar to the magnitude and the timing observed in oxazolidinone-treated cynomolgus macaques (Fig. 3 and fig S6A, B) suggesting that, at least for this class of agent, this model is likely to have predictive validity for human therapeutic utility. The PET/CT data in macaques are validated by measures of bacterial burden. In the non-human primates, the total glycolytic activity correlates reasonably well with lung bacteriologic burden (Fig. S7), which is consistent with the human response data. Thus, our data support that PET/CT imaging can be used to rapidly assess therapeutic response, with the added benefit that single drug treatment is acceptable in animal models, whereas it is not in most human studies. PET/CT offers a valuable bridging tool between animal models and early phase human clinical trials, and the NHP model presents a tractable alternative to explore combination studies with new and existing agents as well as studies of appropriate treatment duration, prior to exposing human subjects to additional risk.

Lastly, our study highlights the dynamic nature of individual lesions in patients with a long-standing history of disease, revealed by scanning subjects in the delayed arm, at study entry and immediately prior to their first dose of LZD. In untreated subjects, this response was highly asynchronous: individual lesions progressed and regressed without any major consistent changes across all lesions. This suggests that the fate of an individual lesion in patients with active disease (without strong drug pressure) is determined locally, and that TB disease, rather than a chronic set of stable lesions, may in fact be much more heterogeneous than initially supposed. This heterogeneity may explain the paradox of the well-documented impact of isoniazid on patients with latent disease despite the complete lack of impact of isoniazid on non-replicating bacilli (31). Isoniazid may simply tip the balance by blocking the development of new lesions while existing lesions cycle through a natural waning that favors the host. We have argued that latent TB infections, in particular, represent a

metastable spectrum ranging from sterile lesions to subclinical disease (32) and these results fit with a dynamic and heterogeneous picture of both latent and active disease. The cynomolgus macaque model faithfully reproduces this heterogeneity and using the quantitative PET/CT imaging measures described in these studies provides a directly translatable means of measuring drug efficacy in human clinical trials.

Materials and Methods

Study Design

Cynomolgus macaques (*Macacca fasicularis*) were infected with *M. tuberculosis* (strain Erdman) via bronchoscope and monitored clinically, as previously described (21, 25). Upon development of active TB, animals were randomly assigned to one of three groups: untreated, LZD, or AZD5847. Animals were followed for two months of treatment and then necropsied. Gross pathology, overall bacterial burden scores, and individual granuloma and thoracic lymph node CFU were calculated as described (21, 25) for treatment response. PET/CT scans were performed at baseline (randomization), 1 and 2 months of treatment. Samples were obtained for analyses using the pre-necropsy PET/CT scan as a roadmap, as previously described (25).

PET/CT scan analysis

Humans: The human linezolid study PET-CT scans were done as a substudy of a previously published larger trial (10) and were analyzed by 1 reader using MIM software (v. 6.1, MIM Software Inc, Cleveland, Ohio, USA). For each patient, individual PET-CT scans were fused together, then co-registered across three time points (−2, 0, 6 months; 0, 1, 6 months; 0, 2, 6 months; or 0, 3, 6 months). To improve further the alignment of the lungs, the first and second scans were each deformed to the third scan. Using the Region Grow tool, a region of interest (ROI) was drawn around the entire lung, which was automatically propagated to all three scans. The ROI was manually refined to include all pulmonary lesions while excluding extrapulmonary structures, including the ribs, mediastinum, and heart. When the scans were not perfectly aligned, extrapulmonary structures were excluded from all scans even if this meant excluding some pulmonary areas in other scans. Once the ROI was drawn, it was contracted by 0.2 cm to ensure that all extrapulmonary structures were excluded. This contracted ROI was then used for all subsequent calculations. Hounsfield unit (HU) and standardized uptake value (SUV) histograms were exported for the contracted ROI at each time point. The HU histograms were analyzed using HU −500 to −100 range to represent “soft” lesions and −100 to +200 range to represent “hard” lesions. To exclude background PET uptake, total glycolytic activity for SUV ≥2 was calculated.

Macaques: PET/CT scan was performed using a microPET Focus 220 preclinical PET scanner (Siemens Molecular Solutions, Knoxville, TN) and clinical 8 slice helical CT scanner (Neurologica Corp, Danvers, MA) as previously described (18). Serial macaque PET/CT scans were performed at baseline, 1, and 2 months after treatment was initiated. Osirix viewer, an open-source PACS workstation and DICOM image viewer, was used for both human and macaque scans analyses. Considering the variable amount of baseline disease in both the human TB patient and macaque scans, the following methods to quantify

areas of FDG avid pathology only and exclude uninvolved lung were used. A whole thoracic cavity ROI was segmented with a threshold of normal lung Hounsfield units (<−200 HU) on CT using a growing region algorithm in the Osirix viewer. A closing tool was used and the ROI manually edited as necessary to include all thoracic cavity pathology. This ROI was transferred to the co-registered PET scan and voxels outside the ROI were set to zero in order to exclude normal, uninfected FDG avid tissue, such as the heart and vertebrae. Mediastinal lymph nodes, confirmed at necropsy, were excluded from the total glycolytic activity analyses of the macaque scans. All regions of FDG avid pathology (SUV > 2.3) were manually selected with the Osirix growing region algorithm and the total glycolytic activity was then computed. As serial PET/CT images were not co-registered, this process was repeated for each scan, and the total glycolytic activity at each time point was calculated. Macaque PET analyses were normalized to resting muscle.

Statistical Analyses

Primary analyses focused on comparisons of AZD and LZD versus control, using the Wilcoxon rank sum statistic to test for significance and a Bonferroni correction. Additional tests were similarly based on non-parametric tests. Significance of clustered data, such as that arising from multiple CFU counts per subject, was determined using the bootstrap (33). Comparisons of longitudinal results were evaluated using permutation-based p-values to ensure appropriate family-wise error rates given the multiple hypothesis tests.

Supplementary Material

Refer to Web version on PubMed Central for supplementary material.

Acknowledgments:

We thank the participants for volunteering for the sub-study of the timing of radiologic response rates to TB chemotherapy as well as the clinical staff of the International Tuberculosis Research Center for their efforts in collecting this data. We thank Astra Zeneca for the kind donation of AZD5847 and for help in selecting an appropriate dose for the non-human primate study. We thank the Dartois lab technical staff, including Matthew Zimmerman and Xiaohua Li, for method development and sample analysis. We also thank the members of the Flynn lab technical staff, who contributed to this study, including Melanie O'Malley, Paul Johnston, Jaime Tomko, Daniel Fillmore, Jim Frye, Mark Rodgers, Carolyn Bigbee, Chelsea Chedrick, and Cathy Cochran.

Funding: Funding for this study was provided by the Intramural Research Program of the NIH, NIAID, by the Ministry of Health and Welfare, Republic of Korea, by the Bill and Melinda Gates Foundation TB Drug Accelerator, and by the National Cancer Institute, NIH, under Contract No. HHSN261200800001E. The content of this publication does not necessarily reflect the views or policies of the Department of Health and Human Services, nor does mention of trade names, commercial products, or organizations imply endorsement by the U.S. Government.

REFERENCES

1. Zumla A, George A, Sharma V, Herbert N, Baroness Masham of I, WHO's 2013 global report on tuberculosis: successes, threats, and opportunities. Lancet 382, 1765–1767 (2013). [PubMed: 24269294]
2. World Health Organization, in Treatment of Tuberculosis: Guidelines. 4th edition. (Geneva, 2010).
3. Christian KA, Ijaz K, Dowell SF, Chow CC, Chitale RA, Bresee JS, Mintz E, Pallansch MA, Wassilak S, McCray E, Arthur RR, What we are watching--five top global infectious disease threats, 2012: a perspective from CDC's Global Disease Detection Operations Center. Emerging health threats journal 6, 20632 (2013). [PubMed: 23827387]

4. Franzblau SG, DeGroote MA, Cho SH, Andries K, Nuermberger E, Orme IM, Mdluli K, Angulo-Barturen I, Dick T, Dartois V, Lenaerts AJ, Comprehensive analysis of methods used for the evaluation of compounds against Mycobacterium tuberculosis. Tuberculosis 92, 453–488 (2012). [PubMed: 22940006]

5. Dartois V, Barry CE, 3rd, A medicinal chemists' guide to the unique difficulties of lead optimization for tuberculosis. Bioorganic & medicinal chemistry letters 23, 4741–4750 (2013). [PubMed: 23910985]

6. Mitchison DA, Chang KC, Experimental models of tuberculosis: can we trust the mouse? American journal of respiratory and critical care medicine 180, 201–202 (2009). [PubMed: 19633156]

7. Coates AR, Hu Y, Jindani A, Mitchison DA, Contradictory results with high-dosage rifamycin in mice and humans. Antimicrobial agents and chemotherapy 57, 1103 (2013). [PubMed: 23341429]

8. Via LE, Lin PL, Ray SM, Carrillo J, Allen SS, Eum SY, Taylor K, Klein E, Manjunatha U, Gonzales J, Lee EG, Park SK, Raleigh JA, Cho SN, McMurray DN, Flynn JL, Barry CE, 3rd, Tuberculous granulomas are hypoxic in guinea pigs, rabbits, and nonhuman primates. Infection and immunity 76, 2333–2340 (2008). [PubMed: 18347040]

9. Eum SY, Kong JH, Hong MS, Lee YJ, Kim JH, Hwang SH, Cho SN, Via LE, Barry CE, 3rd, Neutrophils are the predominant infected phagocytic cells in the airways of patients with active pulmonary TB. Chest 137, 122–128 (2010). [PubMed: 19749004]

10. Lee M, Lee J, Carroll MW, Choi H, Min S, Song T, Via LE, Goldfeder LC, Kang E, Jin B, Park H, Kwak H, Kim H, Jeon HS, Jeong I, Joh JS, Chen RY, Olivier KN, Shaw PA, Follmann D, Song SD, Lee JK, Lee D, Kim CT, Dartois V, Park SK, Cho SN, Barry CE, 3rd, Linezolid for treatment of chronic extensively drug-resistant tuberculosis. The New England journal of medicine 367, 1508–1518 (2012). [PubMed: 23075177]

11. Ippolito JA, Kanyo ZF, Wang D, Franceschi FJ, Moore PB, Steitz TA, Duffy EM, Crystal structure of the oxazolidinone antibiotic linezolid bound to the 50S ribosomal subunit. Journal of medicinal chemistry 51, 3353–3356 (2008). [PubMed: 18494460]

12. Barnhill AE, Brewer MT, Carlson SA, Adverse effects of antimicrobials via predictable or idiosyncratic inhibition of host mitochondrial components. Antimicrobial agents and chemotherapy 56, 4046–4051 (2012). [PubMed: 22615289]

13. Dooley KE, Nuermberger EL, Diacon AH, Pipeline of drugs for related diseases: tuberculosis. Current opinion in HIV and AIDS 8, 579–585 (2013). [PubMed: 24100880]

14. Urbina O, Ferrandez O, Espona M, Salas E, Ferrandez I, Grau S, Potential role of tedizolid phosphate in the treatment of acute bacterial skin infections. Drug design, development and therapy 7, 243–265 (2013).

15. Balasubramanian V, Solapure S, Iyer H, Ghosh A, Sharma S, Kaur P, Deepthi R, Subbulakshmi V, Ramya V, Ramachandran V, Balganesh M, Wright L, Melnick D, Butler SL, Sambandamurthy VK, Bactericidal Activity and Mechanism of Action of AZD5847, a Novel Oxazolidinone for Treatment of Tuberculosis. Antimicrobial agents and chemotherapy 58, 495–502 (2014). [PubMed: 24189255]

16. Wookey A, Turner PJ, Greenhalgh JM, Eastwood M, Clarke J, Sefton C, AZD2563, a novel oxazolidinone: definition of antibacterial spectrum, assessment of bactericidal potential and the impact of miscellaneous factors on activity in vitro. Clinical microbiology and infection : the official publication of the European Society of Clinical Microbiology and Infectious Diseases 10, 247–254 (2004).

17. Lin PL, Dartois V, Johnston PJ, Janssen C, Via L, Goodwin MB, Klein E, Barry CE, 3rd, Flynn JL, Metronidazole prevents reactivation of latent Mycobacterium tuberculosis infection in macaques. Proceedings of the National Academy of Sciences of the United States of America 109, 14188–14193 (2012). [PubMed: 22826237]

18. Lin PL, Coleman T, Carney JP, Lopresti BJ, Tomko J, Fillmore D, Dartois V, Scanga C, Frye LJ, Janssen C, Klein E, Barry CE, 3rd, Flynn JL, Radiologic responses in cynomolgous macaques for assessing tuberculosis chemotherapy regimens. Antimicrobial agents and chemotherapy, (2013).

19. Via LE, Weiner DM, Schimel D, Lin PL, Dayao E, Tankersley SL, Cai Y, Coleman MT, Tomko J, Paripati P, Orandle M, Kastenmayer RJ, Tartakovsky M, Rosenthal A, Portevin D, Eum SY, Lahouar S, Gagneux S, Young DB, Flynn JL, Barry CE, 3rd, Differential virulence and disease

progression following Mycobacterium tuberculosis complex infection of the common marmoset (Callithrix jacchus). Infection and immunity 81, 2909–2919 (2013). [PubMed: 23716617]

20. Lin PL, Pawar S, Myers A, Pegu A, Fuhrman C, Reinhart TA, Capuano SV, Klein E, Flynn JL, Early events in Mycobacterium tuberculosis infection in cynomolgus macaques. Infection and immunity 74, 3790–3803 (2006). [PubMed: 16790751]
21. Lin PL, Rodgers M, Smith L, Bigbee M, Myers A, Bigbee C, Chiosea I, Capuano SV, Fuhrman C, Klein E, Flynn JL, Quantitative comparison of active and latent tuberculosis in the cynomolgus macaque model. Infection and immunity 77, 4631–4642 (2009). [PubMed: 19620341]
22. McGee B, Dietze R, Hadad DJ, Molino LP, Maciel EL, Boom WH, Palaci M, Johnson JL, Peloquin CA, Population pharmacokinetics of linezolid in adults with pulmonary tuberculosis. Antimicrobial agents and chemotherapy 53, 3981–3984 (2009). [PubMed: 19564361]
23. Reele S, Xiao AJ, Das S, Balasubramanian V, Melnick D, paper presented at the 51th ICAAC Interscience Conference on Antimicrobial Agents and Chemotherapy, Chicago, IL, September 17–20, 2011 2011.
24. Reele S, Xiao AJ, Das S, Balasubramanian V, Melnick D, paper presented at the 51th ICAAC Interscience Conference on Antimicrobial Agents and Chemotherapy, Chicago, IL, September 17–20, 2011 2011.
25. Lin PL, Ford CB, Coleman MT, Myers AJ, Gawande R, Ioerger T, Sacchettini J, Fortune SM, Flynn JL, Sterilization of granulomas is common in active and latent tuberculosis despite within-host variability in bacterial killing. Nature medicine 20, 75–79 (2014).
26. Chen RY, Dodd LE, Lee M, Paripati P, Hammoud DA, Mountz JM, Jeon D, Zia N, Zahiri H, Coleman MT, Carroll MW, Lee JD, Jeong YJ, Herscovitch P, Lahouar S, Tartakovsky M, Rosenthal A, Somaiyya S, Lee S, Goldfeder LC, Cai Y, Via LE, Park SK, Cho SN, Barry CE, 3rd, PET/CT Imaging Correlates with Treatment Outcome in Patients with Multi-Drug Resistant Tuberculosis. Sci Trans Med his issue, (2014).
27. Tse-Chang A, Kunimoto D, Der E, Ahmed R, Assessment of linezolid efficacy, safety and tolerability in the treatment of tuberculosis: A retrospective case review. The Canadian journal of infectious diseases & medical microbiology = Journal canadien des maladies infectieuses et de la microbiologie medicale / AMMI Canada 24, e50–52 (2013).
28. Roongruangpitayakul C, Chuchottaworn C, Outcomes of MDR/XDR-TB patients treated with linezolid: experience in Thailand. Journal of the Medical Association of Thailand = Chotmaihet thangphaet 96, 1273–1282 (2013). [PubMed: 24350407]
29. Sotgiu G, Centis R, D'Ambrosio L, Spanevello A, Migliori GB, International L Group for the study of, Linezolid to treat extensively drug-resistant TB: retrospective data are confirmed by experimental evidence. The European respiratory journal 42, 288–290 (2013). [PubMed: 23813314]
30. Chang KC, Yew WW, Cheung SW, Leung CC, Tam CM, Chau CH, Wen PK, Chan RC, Can intermittent dosing optimize prolonged linezolid treatment of difficult multidrug-resistant tuberculosis? Antimicrobial agents and chemotherapy 57, 3445–3449 (2013). [PubMed: 23650165]
31. de Steenwinkel JE, de Knegt GJ, ten Kate MT, van Belkum A, Verbrugh HA, Kremer K, van Soolingen D, Bakker-Woudenberg IA, Time-kill kinetics of anti-tuberculosis drugs, and emergence of resistance, in relation to metabolic activity of Mycobacterium tuberculosis. The Journal of antimicrobial chemotherapy 65, 2582–2589 (2010). [PubMed: 20947621]
32. Barry CE, 3rd, Boshoff HI, Dartois V, Dick T, Ehrt S, Flynn J, Schnappinger D, Wilkinson RJ, Young D, The spectrum of latent tuberculosis: rethinking the biology and intervention strategies. Nature reviews. Microbiology 7, 845–855 (2009). [PubMed: 19855401]
33. Efron B, Tibshirani R, An Introduction to the Bootstrap. (Chapman & Hall/ CRC, 1993).

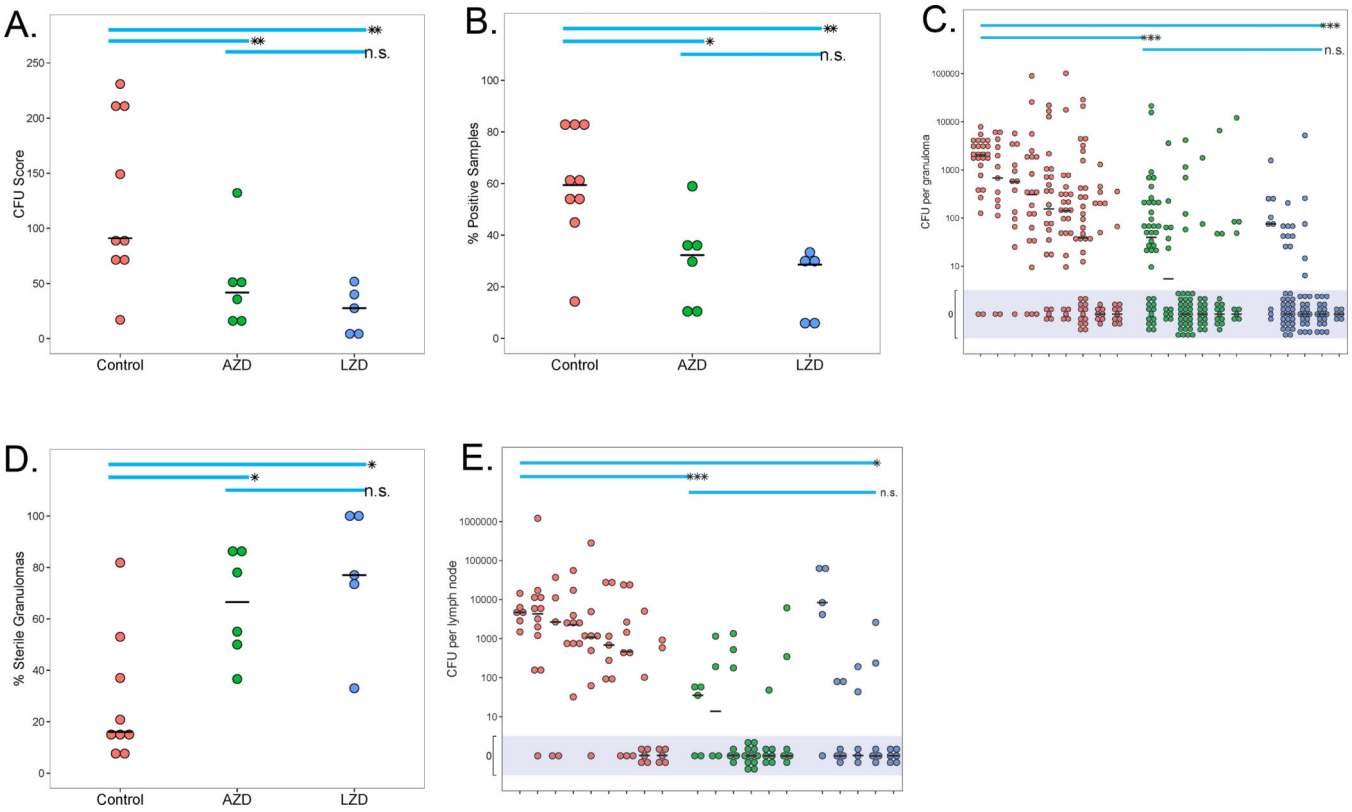

Fig. 1. LZD or AZD5847 treatment reduces bacterial burden in macaques.

(**A**) Overall bacterial burden (CFU score) was lower in LZD- or AZD-treated macaques, compared to untreated controls. CFU score took into account bacterial burden from all grossly visible granulomas and areas of pathology, lymph nodes, extrapulmonary sites, and random lung tissue, as previously described (21). (**B**) This panel shows the percentage of tissue samples (lung tissue, granulomas, lymph nodes, extrapulmonary organs) from each individual animal at necropsy that were positive for Mtb growth. (**C**) Individual granulomas were plated for total CFU (each circle represents a granuloma, each individual animal is shown) and the mean CFU/granuloma (solid line) was calculated; shaded area reflects all those granulomas below level of detection). (**D**) The percentage of granulomas failing to yield any culturable bacilli when plated was reduced by oxazolidinone treatment (each symbol is an individual animal). (**E**) The total CFU within each thoracic lymph node was reduced by LZD or AZD treatment compared to untreated controls (symbols represent each individual thoracic lymph node in each animal). P-values are indicated as follows: * $p<0.05$, ** $p<0.01$, ***$p<0.001$. The short horizontal black line indicates median.

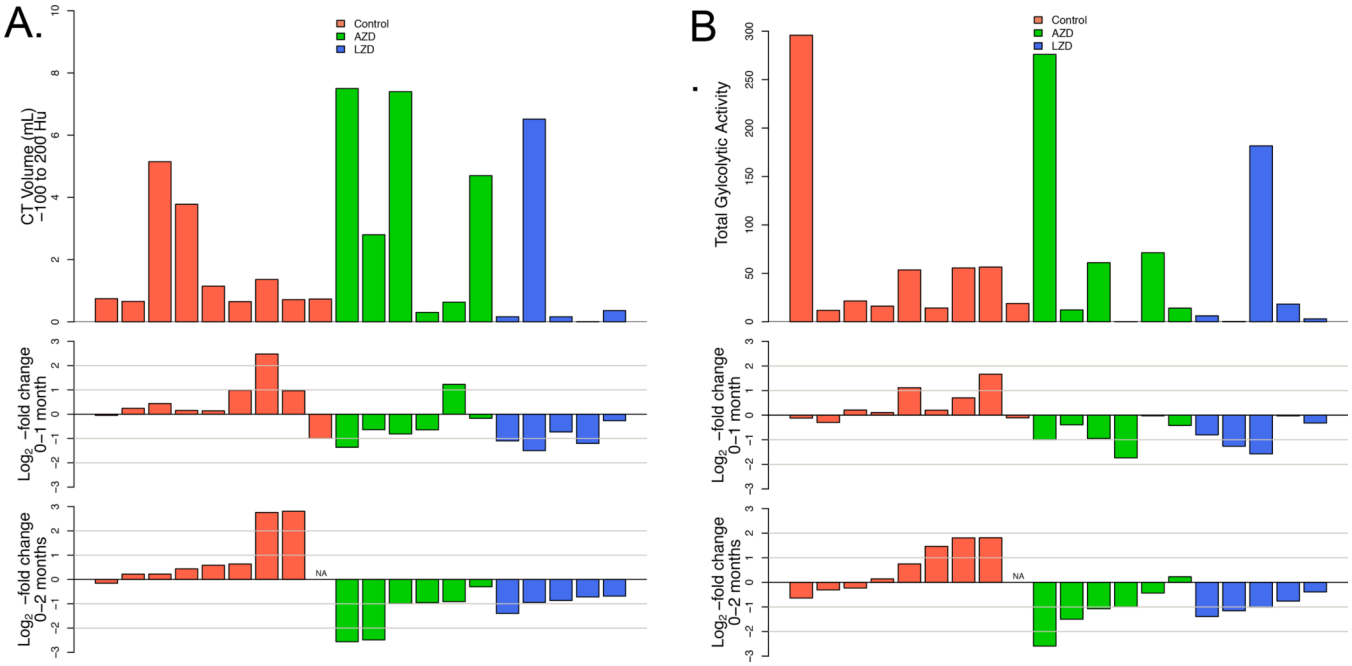

Fig. 2. Radiologic response rates of oxazolidinone-treated animals by treatment group.

(A) Volume of "hard" abnormal CT density (−100 to 200 HU) for each animal at baseline (top panel), $\log_2$-fold change from baseline to one month (middle panel), $\log_2$-fold change from baseline to two months (bottom panel). **(B)** Total glycolytic activity (TGA) for each animal at baseline (top panel), $\log_2$-fold change from baseline to one month (middle panel), $\log_2$-fold change from baseline to two months (bottom panel).

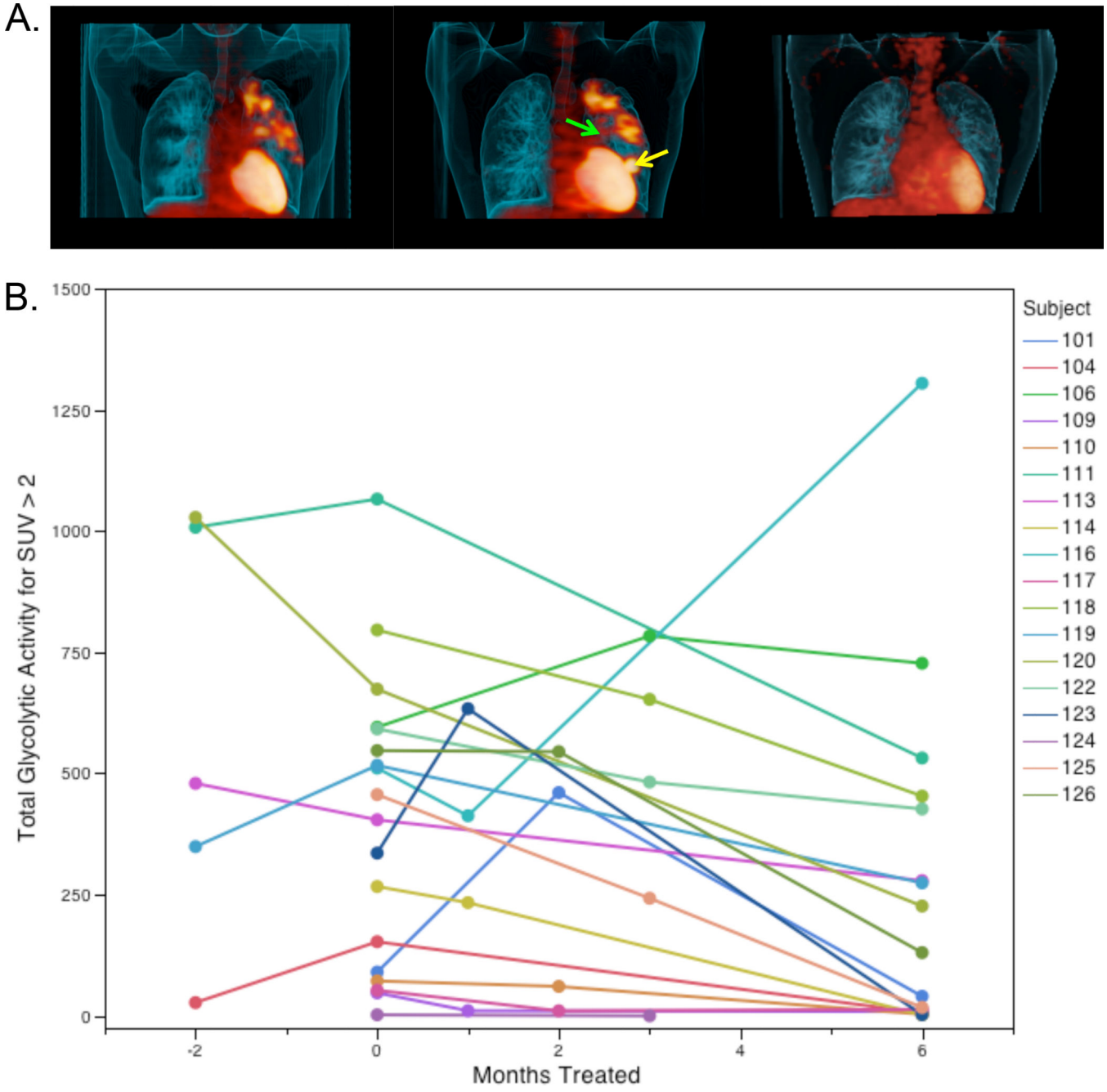

Fig. 3. Radiologic response rates for subjects in the LZD substudy.

(**A**) Representative subject in the delayed arm who was enrolled failing all available therapy and monitored for two months prior to receiving LZD treatment. The left scan shows the FDG PET scan at study entry, the center scan immediately prior to receiving LZD and the right scan after six months of LZD therapy. All scans are shown projected at the same standardized uptake value (SUV). This subject finished two years of LZD therapy and was disease-free at their follow-up visit six months after discontinuing therapy. (**B**) Temporal responses of individual subjects during LZD therapy. Individual subjects received three scans in total and were randomly allocated to different scanning times. "−2" refers to

subjects enrolled in the delayed start arm who received a study entry exam but had no change to their failing regimen and also received a second scan immediately prior to the start of therapy. “0” (on the x-axis) refers to the scan collected prior to administration of LZD (up to one week prior to drug start). Scans were collected within a two-week period of the indicated time point. P=0.005 for the difference in mean total glycolytic activity (TGA) between month 0 and month 6.

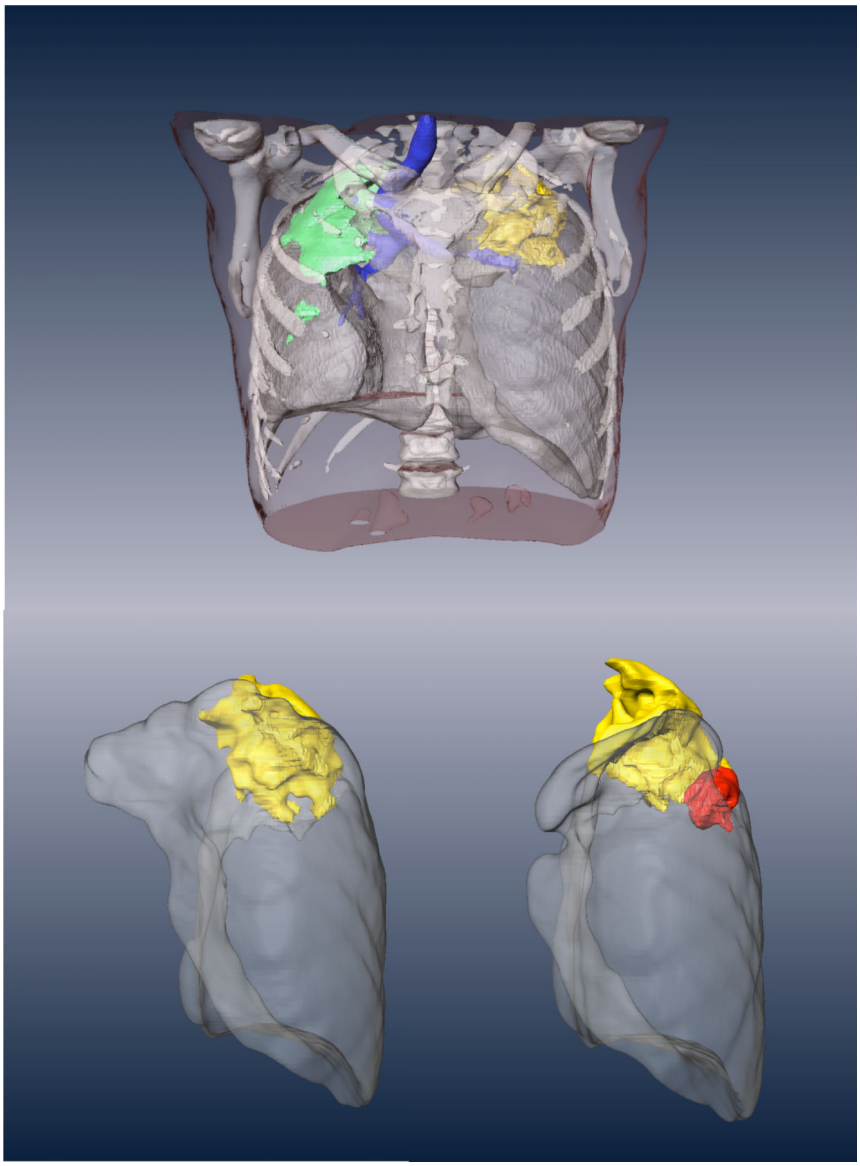

Fig. 4. CT findings of a patient showing an initial response to therapy followed by emergence of LZD resistance.

This subject presented with bilateral, apical disease with the major site of FDG avidity being the left upper lung (yellow and see fig. S5). At one month (left bottom shows the isolated left lung) this site of disease showed a modest reduction in metabolic activity and a slight resolution of CT features consistent with a positive response to therapy but at six months (bottom right) a new lesion (red) emerged anterior and inferior to the initial large apical cavity in the left upper lobe. The patient initially converted their sputum smear and culture to negative but subsequently developed LZD-resistant bacteria that was confirmed genetically to map to the LZD binding site.

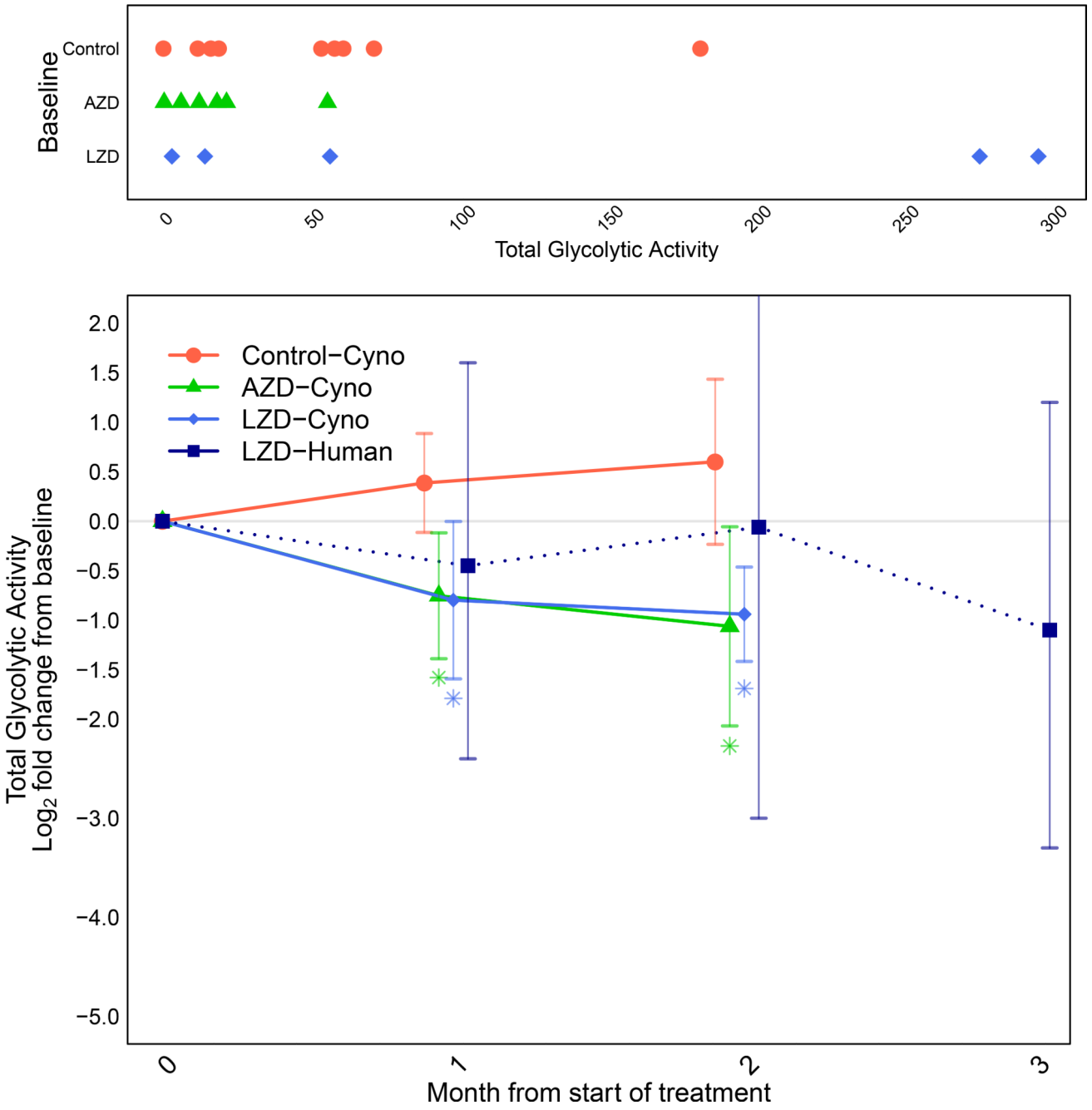

Fig. 5. Comparison of radiologic response rates in humans and macaques by PET.

(Top) Baseline extents of disease in individual animals by treatment group showing the total glycolytic activity (TGA) in all areas of FDG uptake. (**Bottom**) Longitudinal changes in average $\log_2$-fold change (and 95% confidence intervals) in TGA relative to baseline by treatment group for non-human primates and humans (linezolid treatment only). Colored asterisks indicate statistical significance relative to control arm mean (*P<0.05). Dotted line connecting human linezolid values indicates that different subjects were represented by their mean values at months 1, 2 and 3.

Table 1.
Pharmacokinetic parameters of linezolid and AZD5847 in primates.

Shown are pharmacokinetic parameters of linezolid and AZD5847 in cynomolgus macaques and in humans at clinically used doses (linezolid) (22) or projected efficacious doses (AZD5847) (24). C_{max}: peak plasma concentration; T_{max}: time to peak plasma concentration; $AUC_{[0–24]}$: Area Under the Curve from 0 to 24h post-dose; $T_{1/2}$: elimination half-life; q.d.: once daily; b.i.d.: twice daily.

Cynomolgus macaques					**TB patients**				
dose (frequency)	**C_{max}**	**T_{max}**	**$AUC_{[0–24]}$**	**$T_{1/2}$ (elim)**	**dose (frequency)**	**C_{max}**	**T_{max}**	**$AUC_{[0–24]}$**	**$T_{1/2}$ (elim)**
mg/kg	**µg/ml**	**h**	**µg*h/ml**	**h**	**mg**	**µg/ml**	**h**	**µg*h/ml**	
Linezolid									
10 (single dose)	1.8–4.2	4	27–36	5.7–6.3	600 (q.d.)	12–21	1–4	65–125	2.4–3.9
30 (single dose)	14–15	4	121–198	3–4	600 (b.i.d.)	12–25	1–4	80–172	3.0–5.8
AZD5847					**Healthy Volunteers**				
					at steady state	mean (%CV)	range	mean (%CV)	mean (%CV)
10 (single dose)	3.3	4	35–40	5.2–5.4	400 (b.i.d.)	5.9 (12.6)	2–5	48 (15)	8.7 (14.40)
20 (single dose)	1.7–3.2	4–10	23–37	7.7–11.2	800 (b.i.d.)	10.7 (8.6)	2–4	90 (9)	10.0 (21.8)